Meccanica (2013) 48:2349–2366
DOI 10.1007/s11012-013-9753-4

Failure mode transitions in RC beams: A cohesive/overlapping crack model application

A. Carpinteri · M. El-Khatieb · E. Cadamuro

Received: 26 March 2013 / Accepted: 23 April 2013 / Published online: 8 May 2013

Abstract The analysis of reinforced concrete beams in flexure taking into account the nonlinear behaviour of concrete is addressed by a numerical approach based on the Cohesive-Overlapping Crack Model. An extensive experimental research has been proposed by Bosco and Carpinteri (Scale effects and transitional phenomena of reinforced concrete beams in flexure. ESIS Technical Committée 9 Round Robin proposal, 1993), Bosco et al. (Scale effects and transitional failure phenomena of reinforced concrete beams in flexure. Report to ESIS Technical Committée 9, 1996) and El-Khatieb (Transizione di scala duttile-fragile per le travi in calcestruzzo armato. PhD Thesis, 1997) in order to obtain a rational explanation for failure transitional phenomena of RC beams by varying steel percentage and/or beam slenderness and/or beam size-scale. In the present paper, collapse mechanisms due to concrete tensile cracking, concrete compressive crushing and steel yielding and/or slippage are analysed and a numerical vs. experimental comparison is presented in order to validate the proposed model.

Keywords Reinforced concrete beams · Ductile-to-brittle transitions · Size-scale effects · Structural instability · Cohesive crack

A. Carpinteri · E. Cadamuro (✉)
Department of Structural and Geotechnical Engineering, Politecnico di Torino, Corso Duca degli Abruzzi 24, 10129 Torino, Italy
e-mail: erica.cadamuro@polito.it

E. Cadamuro
e-mail: erica.daniela@gmail.com

M. El-Khatieb
Civil Engineering Department, Isra University, P.O. Box 22, Amman, Jordan

1 Introduction

The failure mode of RC beams in flexure is affected by nonlinearities of the constituent materials such as concrete tensile cracking, concrete compressive crushing and steel yielding and/or slippage. Their interaction depends on the mechanical and the geometrical parameters of the beams and will be herein analysed by varying the beam size, the reinforcement percentage and the beam slenderness. In this context, classical approaches, such as Limit Analysis, cannot predict the ductile-to-brittle transition in the failure mode due to the size-scale effects, commonly observed in experimental tests and usually studied by means of fracture mechanics.

The analysis of reinforced concrete beams has been addressed in the literature by several authors mainly by means of two different approaches: Linear Elastic Fracture Mechanics (LEFM) and the Cohesive Crack Model. In the former context, the Bridged Crack Model, which is an analytical model, has been originally proposed by Carpinteri [12, 15] and Bosco and

Carpinteri [4] for RC beams with a single reinforcement layer, where the problem of minimum reinforcement amount has also been investigated [1, 5]. Afterwards, the model has been reformulated by Bosco and Carpinteri [7] and Carpinteri and Massabò [17] for fiber-reinforced concrete members with cohesive closing stresses and extended to the simultaneous presence of both steel bars and fiber reinforcements [19]. More recently, it has been further extended by Carpinteri et al. [21] in order to describe the shear crack propagation, according to the method proposed by Jenq and Shah [34], and subsequently improved by So and Karihaloo [41], for the calculation of the stress-intensity factor at the tip of a shear crack with a nonlinear trajectory. In all the aforementioned applications, this efficient analytical tool, which avoids finite element numerical computations, has permitted to reveal scale effects, instability phenomena and brittle-to-ductile transitions of reinforced structural elements. Clearly, it has to be remarked that LEFM holds only when the size of the fracture process zone at the crack tip is sufficiently small with respect to the size of the crack and the size of the specimen. Otherwise, suitable models, such as the Cohesive Crack Model, have to be used to take into account the nonlinear behaviour in the process zone. Applications of such a model to longitudinally reinforced concrete beams have been proposed in the framework of finite element method since 1985 [27, 28] for a systematic analysis of the diagonal tension failure mode. Different numerical approaches, based on elastic coefficients computed a-priori by means of a finite element analysis, have been proposed by Hawkins and Hjorsetet [29], Ruiz et al. [40], and Brincker et al. [10]. They permitted to investigate the influence of the main parameters on the mechanical response. As an example, Ruiz [39] found that the bond-slip relation between concrete and reinforcement plays a central role in determining the peak load. The higher the bond stresses, the higher the peak load. On the contrary, it does not influence the value of the ultimate resistant moment corresponding to steel yielding and complete disconnection of the concrete cross-section. Brincker et al. [10], instead, put into evidence a brittle-to-ductile transition in the overall failure response by increasing the beam size, for constant values of reinforcement percentage.

Different dimensionless parameters said *brittleness numbers* have been first proposed in the framework of Linear Elastic Fracture Mechanics by Carpinteri, in order to study the stability of progressive cracking in brittle materials [11, 13, 14] and in reinforced concrete elements [12, 15], and to evaluate the minimum reinforcement necessary to avoid unstable crack propagation [5].

In fact, in the case of reinforced concrete elements, a nondimensional parameter has been introduced [12, 15]:

$$N_P = \rho \frac{\sigma_y h^{1/2}}{K_{\mathrm{IC}}}, \tag{1}$$

where ρ and σ_y are, respectively, the percentage and the yielding strength of steel reinforcement. In this case, a ductile-to-brittle transition occurs by decreasing the reinforcement brittleness number, N_P. It is worth noting that N_P has been defined in the context of LEFM, and more precisely, with the parameters of the Bridged Crack Model. For this reason, its extension to nonlinear models usually yielded unsatisfactory results. As an example, Brincker et al. [10], obtained different mechanical responses for beams with different depths and reinforcement ratios, even if the brittleness number was kept constant. Similar remarks can also be done with reference to the experimental results by Bosco et al. [8].

More recently, Dimensional Analysis has been applied to the mechanical behaviour of lightly reinforced concrete beams in the case the fracturing process is modelled by a cohesive crack [24]. In particular, this procedure has been applied to the algorithm proposed by Carpinteri et al. [21, 22] and based on the Cohesive and the Overlapping Crack models. It has been demonstrated that two dimensionless parameters, N_P and s, are responsible for the mechanical response, and not N_P only, as considered so far.

In the present paper, the results of an extensive experimental investigation, planned in a Round Robin [9, 25], proposed by ESIS Technical Committee 9 on Concrete, are presented in order to obtain a rational and unified explanation for the transitions between different collapse mechanisms. These results are then analytically interpreted through the unified Cohesive and Overlapping Crack model [21, 22] and a numerical vs. experimental comparison is presented in order to validate the mentioned model.

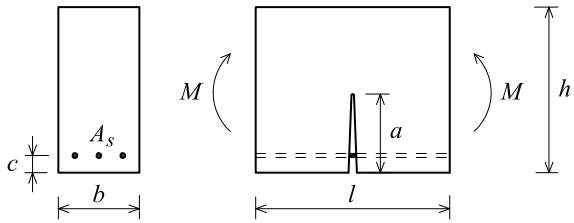

Fig. 1 Scheme of the reinforced concrete element

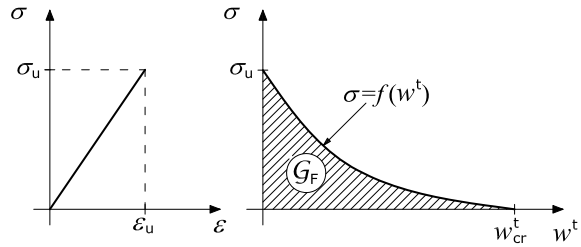

Fig. 2 Cohesive crack model: (**a**) linear-elastic σ–ε law; (**b**) post-peak softening σ–w relationship

2 The integrated cohesive/overlapping crack model

Let us consider the reinforced concrete beam element in Fig. 1 with a rectangular cross-section of thickness b and depth h, a steel reinforcement layer at a distance c from the lower edge and a crack of length a. The beam segment has a length l equal to the depth and is subjected to the bending moment M. We assume that the middle cross-section can be considered as representative of the mechanical behaviour of the whole element, since all the nonlinearities are localized in this section, whereas the outside parts exhibit an elastic response. The structural behaviour of such an element is affected by mechanical nonlinearities due to steel yielding, tensile cracking and compression crushing of concrete. The numerical model herein proposed is the more general algorithm introduced by Carpinteri et al. [21, 22] for modelling the mechanical response of all the possible situations ranging from plain to over-reinforced concrete beams. The proposed model, in fact, permits to correctly describe all the relevant nonlinearities. Similar approaches for implementing a cohesive crack were proposed by Carpinteri ([16], JMPS 1989), Planas and Elices [37], Bazant and Beisel [3], Ruiz et al. [40], and Brincker et al. [10].

2.1 Constitutive models

The mechanical response of concrete in tension is described by the *Cohesive Crack Model* [16, 31], which considers a damaged and micro-cracked process zone ahead of the tip of the real crack, where a part of the macro-crack in evolution partially stitched by inclusions, aggregates or fibres, can be distinguished and where nonlinear and dissipative microscopic phenomena take place. In particular, a linear-elastic stress–strain relationship is assumed for the undamaged phase (see Fig. 2a), whereas a softening stress–crack opening relationship describes the process zone until the critical opening, w^t_{cr}, is reached (see Fig. 2b). The softening function, $\sigma = f(w)$, is considered as a material property, as well as the critical value of the crack opening, w^t_{cr}, and the fracture energy, $\mathcal{G}_F$. The shape of $f(w)$ may vary from linear to bilinear or even more complicated relationships depending on the characteristics of the considered material and the analysed problem. For instance, when plain concrete subjected to an high strain gradient is studied, a simple linear softening law may be sufficient to obtain accurate results (see [18] for a comparison between different shapes of the softening law). On the other hand, bilinear relationships with long tails are necessary to describe fibre-reinforced concrete elements, taking into account the closing stresses exerted by the fibres for large values of crack opening.

As far as modelling of concrete crushing failure is concerned, the *Overlapping Crack Model* introduced by Carpinteri et al. [20, 22] is adopted. According to such an approach, clearly confirmed by experimental results [33, 44], and inspired by the pioneering work by Hillerborg [30], the inelastic deformation in the post-peak regime is described by a fictitious interpenetration of the material, while the remaining part of the specimen undergoes an elastic unloading. Such a model differs from others previously proposed, which assume that strain localization takes place within a zone with an extension dependent on the specimen sizes and/or the stress level [2, 33, 35, 36]. A pair of constitutive laws for concrete in compression is introduced, in close analogy with the *Cohesive Crack Model*: a stress-strain relationship until the compressive strength is achieved (Fig. 3a), and a stress relative displacement (*overlapping*) relationship describing the phenomenon of concrete crushing and expulsion (Fig. 3b). The latter law, usually assumed as a

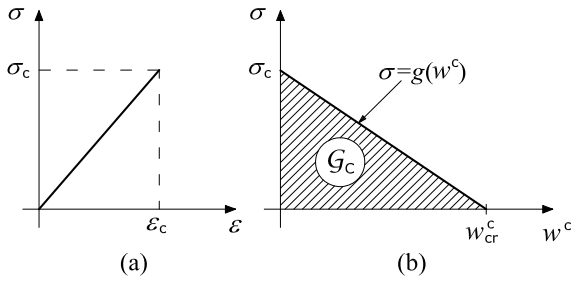

Fig. 3 Overlapping crack model: (**a**) linear-elastic σ–ε law; (**b**) post-peak softening σ–w relationship

linear decreasing function, describes how the stress in the damaged material decreases from its maximum value down to zero as the fictitious interpenetration increases from zero to the critical value, w^c_{cr}. It is worth noting that the crushing energy, $\mathcal{G}_{\mathrm{C}}$, which is a dissipated surface energy, defined as the area below the post-peak softening curve in Fig. 4b, can be assumed as a true material property, since it is not affected by the structural size. An empirical equation for calculating the crushing energy has been recently proposed by Suzuki et al. [42], taking into account the concrete confined compressive strength by means of the stirrups yield strength and the stirrups volumetric content. By varying the concrete compressive strength from 20 to 90 MPa, the crushing energy ranges from 30 to 58 N/mm. The critical value for the crushing interpenetration is experimentally found to be approximately equal to $w^c_{\mathrm{cr}} \approx 1$ mm (see also [33]). It is worth noting that this value is a decreasing function of the compressive strength, in agreement with the more brittle response exhibited by high strength concrete. On the contrary, we observe that, in the case of concrete confinement, the crushing energy, and the corresponding critical value for crushing interpenetration, considerably increases. In relation to both compression strength and critical interpenetration, an increase by approximately one order of magnitude produces an increase in the crushing energy by two orders of magnitude.

The steel reinforcement contribution is modeled by a stress vs. crack opening relationship obtained by means of preliminary studies carried out on the interaction between the reinforcing bar and the surrounding concrete. On the basis of the bond-slip relationship provided by the Model Code 90 [23], and by imposing equilibrium and compatibility conditions, it is possible to correlate the reinforcement reaction to the relative

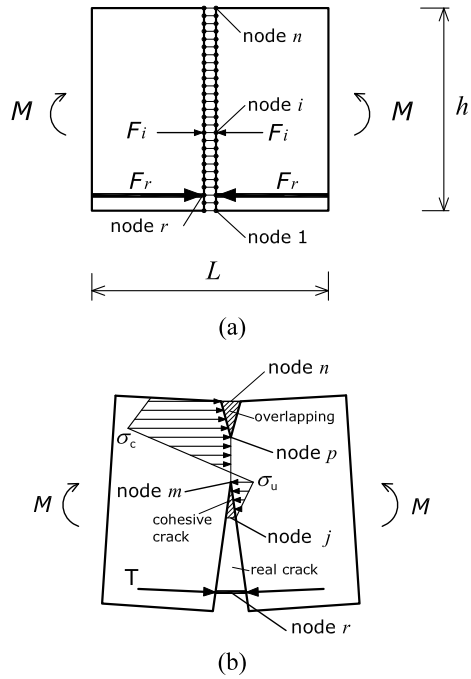

Fig. 4 Finite element nodes (**a**); and force distribution with cohesive crack in tension, crushing in compression and reinforcement closing forces (**b**) across the mid-span cross-section

slip at the crack edge, which corresponds to half the crack opening displacement. Typically, the obtained relationship is characterized by an ascending branch up to steel yielding, to which corresponds a critical value of the crack opening, w_y. After that, the steel reaction is nearly constant. In the present algorithm, this stress-displacement law for steel has been introduced together with the cohesive and overlapping constitutive laws for concrete.

2.2 Numerical algorithm

A suitable algorithm, based on the finite element method, is herein developed to study the mechanical response of the two half-beams. The mid-span cross-section is subdivided into n nodes, where cohesive and overlapping stresses are replaced by equivalent nodal forces, F_i, which depend on the corresponding relative nodal displacements according to the cohesive or overlapping post-peak laws (Fig. 4a). These horizontal forces can be computed as follows:

$$\{F\} = [K_w]\{w\} + \{K_M\}M \tag{2}$$

where $\{F\}$ is the vector of the nodal forces, $[K_w]$ is the matrix of the coefficients of influence for the

nodal displacements, $\{w\}$ is the vector of the nodal displacements, $\{K_M\}$ is the vector of the coefficients of influence for the applied moment, M. Equation (2) permits to study the fracturing and crushing phenomena, computing *a priori*, by a finite element analysis, all the coefficients of influence. For symmetry, only half-element is discretized through quadrilateral plane stress elements with uniform nodal spacing. Then, horizontal constraints are applied on the nodes along the vertical symmetry edge. Each coefficient of influence, $K_w^{i,j}$, which relates the nodal force, F_i, to the nodal displacement, w_j, is computed by imposing a unitary displacement to the corresponding constrained node. On the other hand, each coefficient K_M^i is computed by imposing a unitary external bending moment.

For the generic situation reported in Fig. 4b, the following equations hold:

$$F_i = 0; \quad \text{for } i = 1, 2, \ldots, (j-1);\ i \neq r \tag{3a}$$

$$F_i = f\left(w_i^t\right); \quad \text{for } i = j, \ldots, (m-1);\ i \neq r \tag{3b}$$

$$w_i = 0; \quad \text{for } i = m, \ldots, p \tag{3c}$$

$$F_i = g\left(w_i^c\right); \quad \text{for } i = (p+1), \ldots, n \tag{3d}$$

$$F_i = h(w_i); \quad \text{for } i = r \tag{3e}$$

where: node 1 is at the bottom of the crack face, j corresponds to the real crack tip, m represents the fictitious crack tip, p is the overlapping zone tip, and r corresponds to the reinforcement layer level. Equations (3b), (3d) and (3e) are the constitutive laws of cohesive crack, overlapping crack and steel reinforcement, respectively.

Equations (2) and (3a), (3b), (3c), (3d), (3e) constitute a linear algebraic system of $(2n)$ equations in $(2n+1)$ unknowns, namely $\{F\}$, $\{w\}$ and M. The necessary additional equation derives from the strength criterion adopted to govern the propagation processes. We can set either the force in the fictitious crack tip, m, equal to the ultimate tensile force, F_u, or the force in the crushing zone tip, p, equal to the ultimate compressive force, F_c. It is important to note that cracking and crushing phenomena are physically independent of each other. As a result, the situation which is closer to one of these two possible conditions is chosen to establish the prevailing phenomenon. The driving parameter of the process is the position of the tip that in the considered step has reached the limit resistance. Only this tip is moved to the next node, when passing to the next step. Finally, at each step, we can compute the rotation, ϑ, as follows:

$$\vartheta = \{D_w\}^{\mathcal{T}}\{w\} + D_M M, \tag{4}$$

where D_w^i is the coefficient of influence for the i-th nodal displacement given as the rotation of the free edge corresponding to a unitary horizontal displacement of the i-th node, and D_M is the rotation for the applied bending moment, $M = 1$.

The size-scale effects are taken into account by relationships of proportionality that affect the coefficients of influence entering Eqs. (2) and (4), so that it is not necessary to repeat the finite element analysis for any different beam size. Therefore, if the depth, h, the element length, l, and the thickness, b, are multiplied by a factor k, the coefficients change as follows:

$$K_w^{i,j}(kd) = kK_w^{i,j}(d), \tag{5a}$$

$$K_M^i(kd) = \frac{1}{k}K_M^i(d), \tag{5b}$$

$$D_w^i(kd) = \frac{1}{k}D_w^i(d), \tag{5c}$$

$$D_M(kd) = \frac{1}{k^3}D_M(d). \tag{5d}$$

3 Experimental investigation

The experimental investigation herein considered was carried out by Bosco and Carpinteri in 1996 at the Department of Structural Engineering and Geotechnics of the Politecnico di Torino [9]. These tests were planned in a Round Robin proposed by Bosco and Carpinteri [6], according to an extensive experimental research within ESIS Technical Committee 9 on concrete, in order to obtain a rational and unified explanation for the transitions usually obtained between different collapse mechanisms. 45 reinforced concrete beams were planned to be tested by varying scale, percentage of reinforcement and slenderness, in order to evaluate the dependence of rotational capacity, minimum reinforcement and transitional phenomena of collapse on the beam size-scale. Only 35 specimens were effectively tested.

Three different size-scales (A) 100×100 mm, (B) 100×200 mm and (C) 200×400 mm, and five different tensile reinforcement percentages $\rho = 0.12$ %, 0.25 %, 0.50 %, 1.0 % and 2.0 % were considered (see Fig. 5). The beams, characterized by an effective to total depth ratio $d/h = 0.9$, were subjected to a

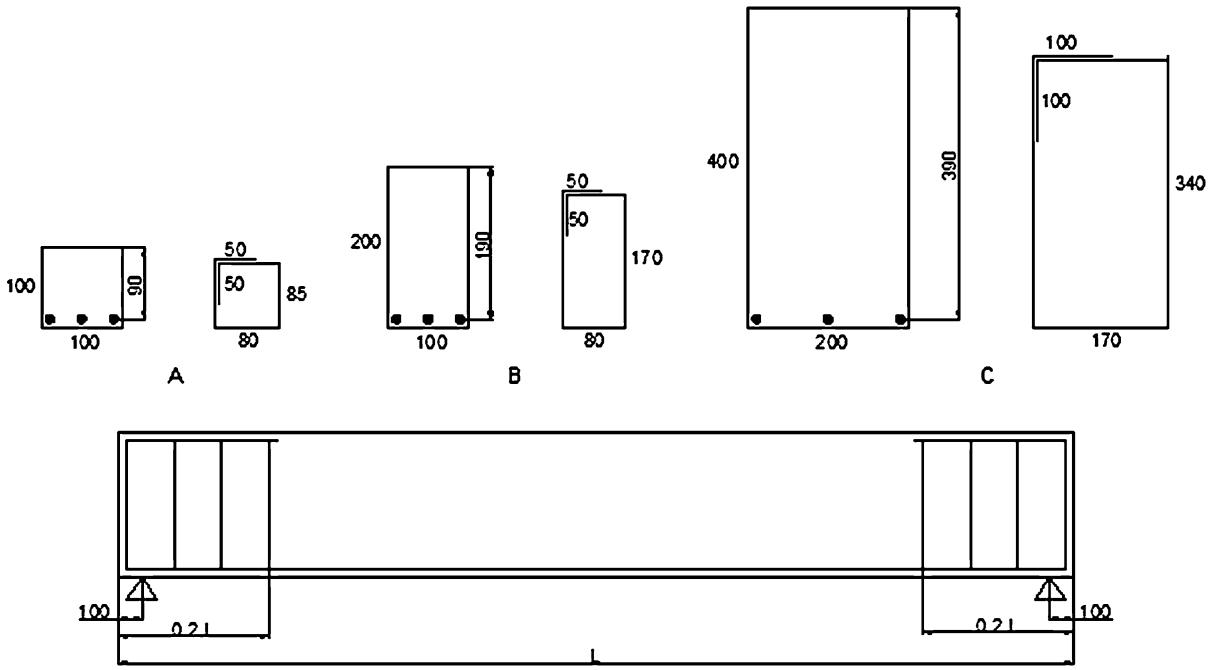

Fig. 5 Geometry and reinforcement of the specimens

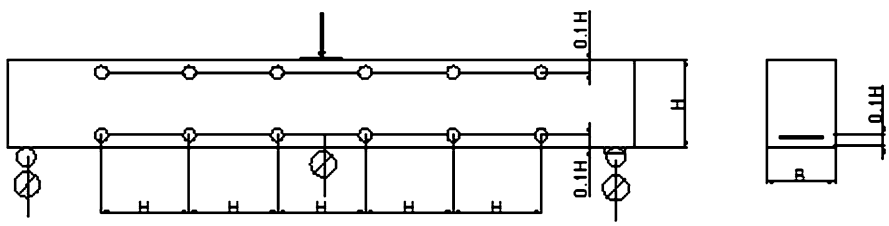

Fig. 6 Testing geometry

three-point bending test. All the beams were realized with the same concrete cast and no shear reinforcement (stirrups) were utilized.

3.1 Testing equipment

A servo-controlled closed-loop machine for tests was used, and in order to avoid a sudden rupture during the possible snap-back phenomenon, in the case of beams with a reinforcement percentage lower than 0.50 %, tests were carried out through a Crack Mouth Opening Displacement Control (CMOD), whereas the other beams have been tested through a displacement control.

Strains at the upper and lower beam edges were measured through potentiometric transducers with a length equal to the beam height, positioned at 1/10 of the beam height from both beam extrados and intrados (Fig. 6). Measurement range of the transducers was of 20 mm. Vertical displacements were measured by means of one or two transducers positioned in the middle of the beam, moreover two additional transducers were utilized in order to catch the settlements in correspondence of the supports and, therefore, to obtain the effective values of the beam displacements.

Supports have been realized by a fixed hinge and a roller permitting horizontal displacements of the beam, as is illustrated in Fig. 6. The load was transferred to the beam by means of a steel plate with a length equal to half the beam height in order to reduce the stress concentration.

Table 1 Experimental values of fracture energy

Weight [g]	Addit. weight [g]	L [mm]	h [mm]	Width b [mm]	Span L [mm]	Initial crack a [mm]	s [mm]	Area diag. [daN mm]	$\mathcal{G}_F$ [N/m]
20460	1406	859	100	102	800	49.0	3.2	44.92	132.2
20090	1406	857	100	104	800	49.0	3.2	34.35	100.5
20380	1406	855	102	100	800	48.5	3.2	40.13	114.4
20810	1406	857	100	105	800	51.5	3.2	33.78	102.3
19705	1406	857	100	100	800	51.0	3.2	37.34	123.2
19900	1406	857	101	101	800	51.9	3.2	36.38	116.3

Table 2 Experimental values of concrete elastic modulus

No	$P1$ [daN]	$P2$ [daN]	$L1$ [mm]	$L2$ [mm]	L [mm]	A [cm^2]	σ [daN/cm^2]	$\varepsilon = \Delta l/l$	E_c [daN/cm^2]
1	10043	3101	0.032	0.012	100	100	69.413	2.04E–04	340257.4
2	10024	3088	0.030	0.011	100	100	69.363	1.96E–04	353890.3
3	10018	3070	0.029	0.010	100	100	69.475	1.94E–04	358118.6
4	9955	3070	0.031	0.012	100	100	68.850	1.97E–04	349492.4

3.2 Experimental determination of materials properties

Additional tests were carried out in order to characterize the cementitious material: 6 concrete beams $100 \times 100 \times 840\ \text{mm}^3$ were subjected to the RILEM standard test [38] for the determination of concrete fracture energy, 4 prisms $100 \times 100 \times 300\ \text{mm}^3$ were subjected to a compressive test for the determination of concrete elastic modulus, and 7 concrete cubes $100 \times 100 \times 100\ \text{mm}^3$ were subjected to a standard test of compression for the determination of concrete compressive strength.

The RILEM Recommendation specifies a method for mortar and concrete by means of stable three-point bending tests on notched beams. It consists in measuring the energy absorbed for separating the specimen into two parts. The fracture energy is defined as the amount of energy necessary to create one unit area of a crack, which is defined as the projected area on a plane parallel to the main crack direction.

Once the energy W_0, represented by the area under the load-displacement curve, has been measured, as well as the displacement δ_0 at final fracture, the fracture energy can be calculated from the equation:

$$\mathrm{G}_F = (W_0 + mg\delta_0)/A_{lig}, \tag{6}$$

Table 3 Experimental results of compressive tests on concrete cubes

Specimen	Load max, $P_{\max}$ [kN]	Unitary strength [N/mm^2]
1	574	57.4
2	552	55.2
3	394	39.4
4	412	41.2
5	434	43.4
6	494	49.4
7	534	53.4

where: $m = m_1 + 2m_2$ with m_1 the weight of the beam between the supports and m_2 the weight of the part of the loading arrangement which is not attached to the machine but follows the beam until failure, g is the acceleration due to gravity, 9.81 m/s^2, δ_0 is the displacement at the final failure of the beam, A_{lig} is the area of the ligament which is the integer cross-section. The average values of $\mathcal{G}_F$ are reported in Table 1, where the quantity $mg\delta_0$ is assumed to be negligible.

An empirical equation for calculating the crushing energy, $\mathcal{G}_c$, has been recently proposed by Suzuki et al. [42], taking into account the concrete confined compressive strength by means of the stirrups yield

Table 4a Geometrical and mechanical properties of specimens size A

	b [mm]	h [mm]	ℓ [mm]	d' [mm]	Nodo d' [–]	A_s [–]	ρ [–]
A012-06	100	100	600	10	16	1Ø5	0.00196
A025-06	100	100	600	10	16	2Ø5	0.0039
A100-06	100	100	600	10	16	2Ø8	0.01
A200-06	100	100	600	10	16	4Ø8	0.02
A012-12	100	100	1200	10	16	1Ø5	0.00196
A025-12	100	100	1200	10	16	2Ø5	0.0039
A050-12	100	100	1200	10	16	1Ø8	0.005
A100-12	100	100	1200	10	16	2Ø8	0.01
A200-12	100	100	1200	10	16	4Ø8	0.02
A025-18	100	100	1800	10	16	2Ø5	0.00196
A050-18	100	100	1800	10	16	1Ø8	0.005
A100-18	100	100	1800	10	16	2Ø8	0.01
A200-18	100	100	1800	10	16	4Ø8	0.02

	R_c [N/mm^2]	E_c [N/mm^2]	$\mathcal{G}_{Ft}$ [N/mm]	f_y [N/mm^2]	E_s [N/mm^2]	f_c [N/mm^2]	f_t [N/mm^2]	$\mathcal{G}_{Fc}$ [N/mm]
A012-06	48.2	10000	0.115	604	210000	40.0	3.0	30
A025-06	48.2	10000	0.115	604	210000	40.0	3.0	30
A100-06	48.2	10000	0.115	643	210000	40.0	3.0	30
A200-06	48.2	10000	0.115	643	210000	40.0	3.0	30
A012-12	48.2	10000	0.115	604	210000	40.0	3.0	30
A025-12	48.2	10000	0.115	604	210000	40.0	3.0	30
A050-12	48.2	10000	0.115	643	210000	40.0	3.0	30
A100-12	48.2	10000	0.115	643	210000	40.0	3.0	30
A200-12	48.2	10000	0.115	643	210000	40.0	3.0	30
A025-18	48.2	10000	0.115	604	210000	40.0	3.0	30
A050-18	48.2	10000	0.115	643	210000	40.0	3.0	30
A100-18	48.2	10000	0.115	643	210000	40.0	3.0	30
A200-18	48.2	10000	0.115	643	210000	40.0	3.0	30

strength and the stirrups volumetric content. Therefore, the following equations are proposed for the crushing energy:

$$\frac{\mathcal{G}_{Fc}}{\sigma_{c0}} = \frac{\mathcal{G}_{Fc0}}{\sigma_{c0}} + 10000 \cdot \frac{k_a^2 \cdot p_e}{\sigma_{c0}^2} \tag{7}$$

$$\mathcal{G}_{Fc0} = 80 - 50k_b \tag{8}$$

$$k_b = 40/\sigma_{c0} \leq 1.0 \tag{9}$$

where $\mathcal{G}_{Fc0}$ is the crushing energy for unconfined concrete, σ_{c0} is the unconfined concrete compressive strength, p_e is the effective lateral pressure, k_a is a confinement coefficient which depends on the strength and content of stirrups.

The concrete crushing energy for unconfined concrete was determined obtaining an average value of 30 N/mm.

The material Young's modulus, E_c, has been evaluated as secant modulus in compression between two stresses after a determined number of loading cycles,

Table 4b Geometrical and mechanical properties of specimens size B

	b [mm]	h [mm]	ℓ [mm]	d' [mm]	Nodo d' [–]	A_s [–]	ρ [–]
B025-06	100	200	1200	20	16	1Ø8	0.0025
B050-06	100	200	1200	20	16	2Ø8	0.005
B100-06	100	200	1200	20	16	4Ø8	0.01
B200-06	100	200	1200	20	16	2Ø16	0.02
B025-12	100	200	2400	20	16	1Ø8	0.0025
B100-12	100	200	2400	20	16	4Ø8	0.01
B200-12	100	200	2400	20	16	2Ø16	0.02

	R_c [N/mm^2]	E_c [N/mm^2]	$\mathcal{G}_{Ft}$ [N/mm]	f_y [N/mm^2]	E_s [N/mm^2]	f_c [N/mm^2]	f_t [N/mm^2]	$\mathcal{G}_{Fc}$ [N/mm]
B025-06	48.2	10000	0.115	643	210000	40.0	3.0	30
B050-06	48.2	10000	0.115	643	210000	40.0	3.0	30
B100-06	48.2	10000	0.115	643	210000	40.0	3.0	30
B200-06	48.2	10000	0.115	518	210000	40.0	3.0	30
B025-12	48.2	10000	0.115	643	210000	40.0	3.0	30
B100-12	48.2	10000	0.115	643	210000	40.0	3.0	30
B200-12	48.2	10000	0.115	518	210000	40.0	3.0	30

namely, until the strain gauges readings are stabilized [43]. E_c can be calculated through the expression:

$$E_c = \Delta\sigma/\Delta\varepsilon \tag{10}$$

where: $\Delta\sigma = \Delta P/A$, with ΔP is the difference between maximum and minimum load in a stabilized cycle and A is the specimen cross section, $\Delta\varepsilon = \Delta l/L$, Δl being the difference between the two values of displacement corresponding to the previous loads and L is the base of measure of the transducer (100 mm). The values of E_c are reported in Table 2.

Concrete compressive strength, f_c, has been obtained from compression standard tests on concrete cubes $100 \times 100 \times 100$ mm. The single and average values are reported in Table 3, where P_c is the resistant crushing force, A_c the cube cross-section area, R_c the cubic compressive strength and f_c the cylindrical compressive strength, with $f_c = 0.83R_c$.

According to Eurocode 2 [26], the concrete flexural strength, f_t, is determined from the following expression, which depends on the mean value of the cylindrical compressive strength:

$$f_t = 1.4\big((f_c - 8)/10\big)^{3/2} \tag{11}$$

The average value is 3.0 N/mm^2.

Summarizing, concrete compressive strength, obtained by 7 cubic specimens with a side equal to 100 mm, presents a mean value equal to 48.2 N/mm^2, concrete elastic modulus, obtained by 4 specimens of $100 \times 100 \times 300$ mm, presents a mean value equal to 35000 N/mm^2 and, finally, concrete fracture energy, determined according to RILEM (RILEM TC50-FMC) on 6 specimens, is characterized by a mean value of 0.115 N/mm. Therefore, the critical value of the concrete fracture toughness, according to the fundamental relationship proposed by Irwin [32], is:

$$K_{IC} = \sqrt{G_{Ft}E_c} = 59.2\ \mathrm{N\,mm^{-3/2}} \tag{12}$$

As regards steel reinforcement, it has been constituted by bars of 5, 8, 16 and 20 mm of nominal diameter. 5 mm diameter bars have not been shown a clear yielding point and, therefore, a conventional limit has been assumed, from the 0.2 % of plastic strain of the material stress-strain curve, equal to 604 N/mm^2. Moreover, the yielding strength of 8, 16 and 20 mm bars, resulted 643, 518 and 567 N/mm^2, respectively. In Tables 4a, 4b and 4c the geometrical characteristics of the beams and the reinforcement percentages are reported together with the mechanical properties of the materials.

Table 4c Geometrical and mechanical properties of specimens size C

	b [mm]	h [mm]	ℓ [mm]	d' [mm]	Nodo d' [–]	A_s [–]	ρ [–]
C012-06	200	400	2400	40	16	2Ø8	0.0012
C025-06	200	400	2400	40	16	4Ø8	0.0025
C050-06	200	400	2400	40	16	2Ø16	0.005
C100-06	200	400	2400	40	16	4Ø16	0.01
C200-06	200	400	2400	40	16	5Ø20	0.02
C012-12	200	400	4800	40	16	2Ø8	0.0012
C100-12	200	400	4800	40	16	4Ø16	0.01
C200-12	200	400	4800	40	16	5Ø20	0.02
C012-18	200	400	7200	40	16	2Ø8	0.0012
C050-18	200	400	7200	40	16	2Ø16	0.005
C100-18	200	400	7200	40	16	4Ø16	0.01
C200-18	200	400	7200	40	16	5Ø20	0.02

	R_c [N/mm^2]	E_c [N/mm^2]	$\mathcal{G}_{Ft}$ [N/mm]	f_y [N/mm^2]	E_s [N/mm^2]	f_c [N/mm^2]	f_t [N/mm^2]	$\mathcal{G}_{Fc}$ [N/mm]
C012-06	48.2	10000	0.115	643	210000	40.0	3.0	30
C025-06	48.2	10000	0.115	643	210000	40.0	3.0	30
C050-06	48.2	10000	0.115	518	210000	40.0	3.0	30
C100-06	48.2	10000	0.115	518	210000	40.0	3.0	30
C200-06	48.2	10000	0.115	567	210000	40.0	3.0	30
C012-12	48.2	10000	0.115	643	210000	40.0	3.0	30
C100-12	48.2	10000	0.115	518	210000	40.0	3.0	30
C200-12	48.2	10000	0.115	567	210000	40.0	3.0	30
C012-18	48.2	10000	0.115	643	210000	40.0	3.0	30
C050-18	48.2	10000	0.115	518	210000	40.0	3.0	30
C100-18	48.2	10000	0.115	518	210000	40.0	3.0	30
C200-18	48.2	10000	0.115	567	210000	40.0	3.0	30

Since the proposed model assumes a linear-elastic perfectly-plastic constitutive law, the yielding strength, f_y, has been assumed equal to the ultimate strength, f_u, and has been varied with the bar diameters according to Table 5. This is necessary to predict the correct ultimate load for steel reinforcement failure. The steel elastic modulus was set $E_s = 210000$ MPa.

4 Numerical results

A comparison between numerical predictions and experimental results, in terms of applied load vs. mid-span deflection curves, is shown in Figs. 7, 8 and 9. In the numerical simulations the RC element of Fig. 4a is assumed to be representative of the mid-span portion of the beam subjected to three-point-bending test. As a result, the mid-span deflection is obtained as the sum of the contribution of the localized rotation given by Eq. (4) and the elastic contribution, according to the following expression:

$$\delta = \delta_{loc} + \delta_{el} = \frac{\vartheta L}{4} + \frac{1}{48}\frac{PL^3}{E_c I}, \tag{13}$$

where L is the beam span, and I is the moment of inertia of the cross-section.

Table 5 Mechanical steel properties

ϕ [mm]	P_y [daN]	P_r [daN]	σ_s [N/mm^2]	ΔL [mm]	Length [mm]	Weight [g]
8	3300	3500	656	6.7	394	156
8	3225	3410	641	6.4	393	155
8	3210	3450	638	6.2	398	157
8	3210	3440	638	6	392	155
5	1215	1390	608.6	3.3	402	63
5	1200	1300	601	3.2	413	65
16	10020	14380	525	17.1	694	1040
16	10200	14330	534.3	17.3	714	1070
16	9450	14320	495	18.2	687	1030
20	17400	19610	583	24.6	611	1430
20	16800	19760	559.5	22	716	1670
20	16800	19610	559.5	23.3	611	1430

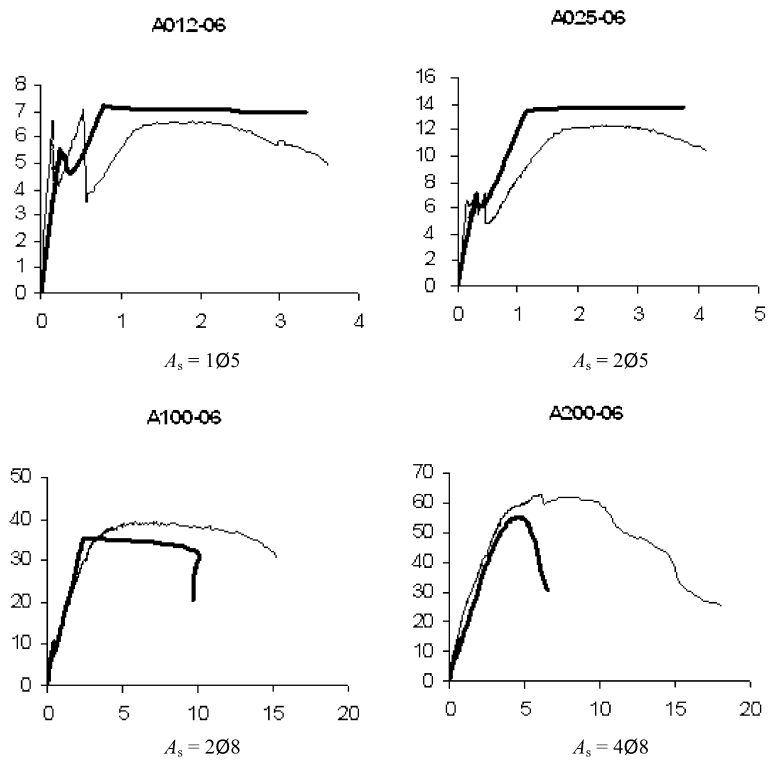

(a)

Fig. 7 Numerical (*thicker curve*) vs. experimental P [kN]–δ [mm] curves for specimens size A: (**a**) $l/h = 6$; (**b**) $l/h = 12$; (**c**) $l/h = 18$

The value of the elastic modulus adopted in the simulations has been set up in order to optimize the numerical-experimental comparisons in the case of the beams with the lowest reinforcement ($\rho = 0.12$ %, 0.25 %). In particular, $E_c = 10000\,\mathrm{N/mm^2}$ has been assumed for all the considered beams, cast by con-

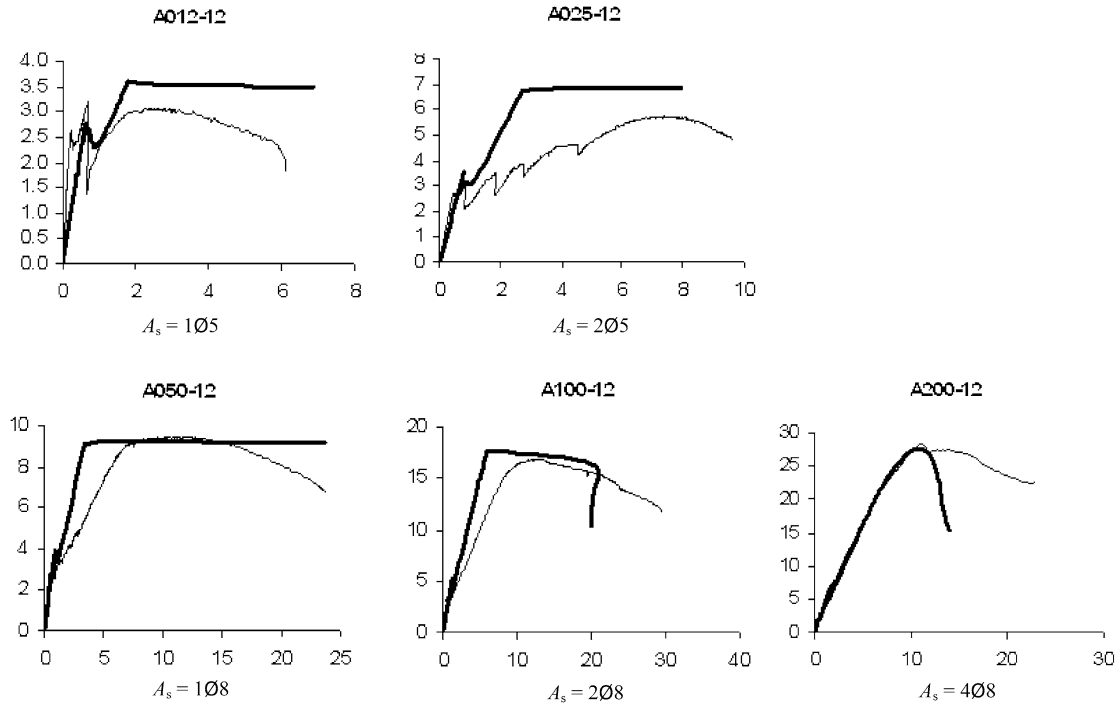

(b)

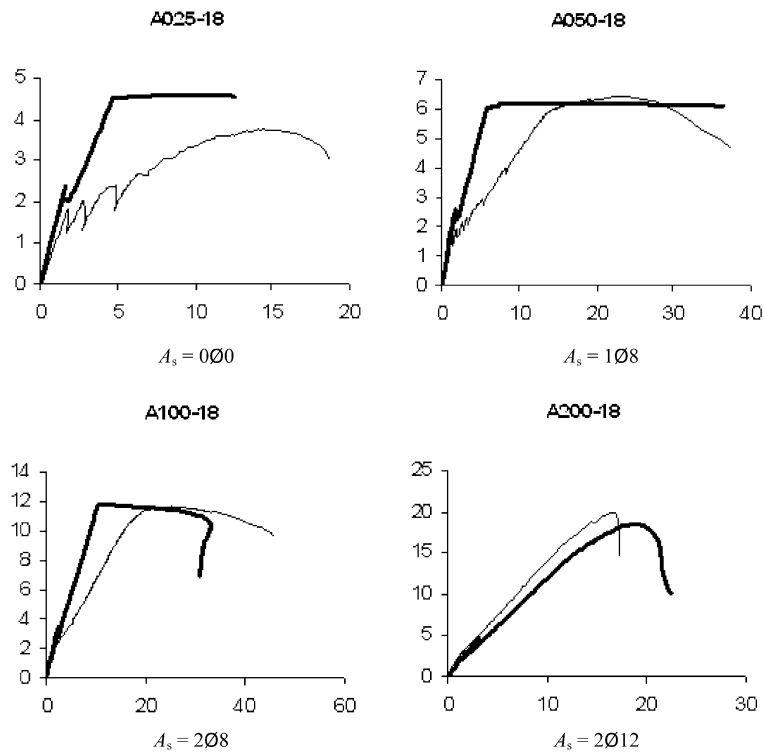

(c)

Fig. 7 (*Continued*)

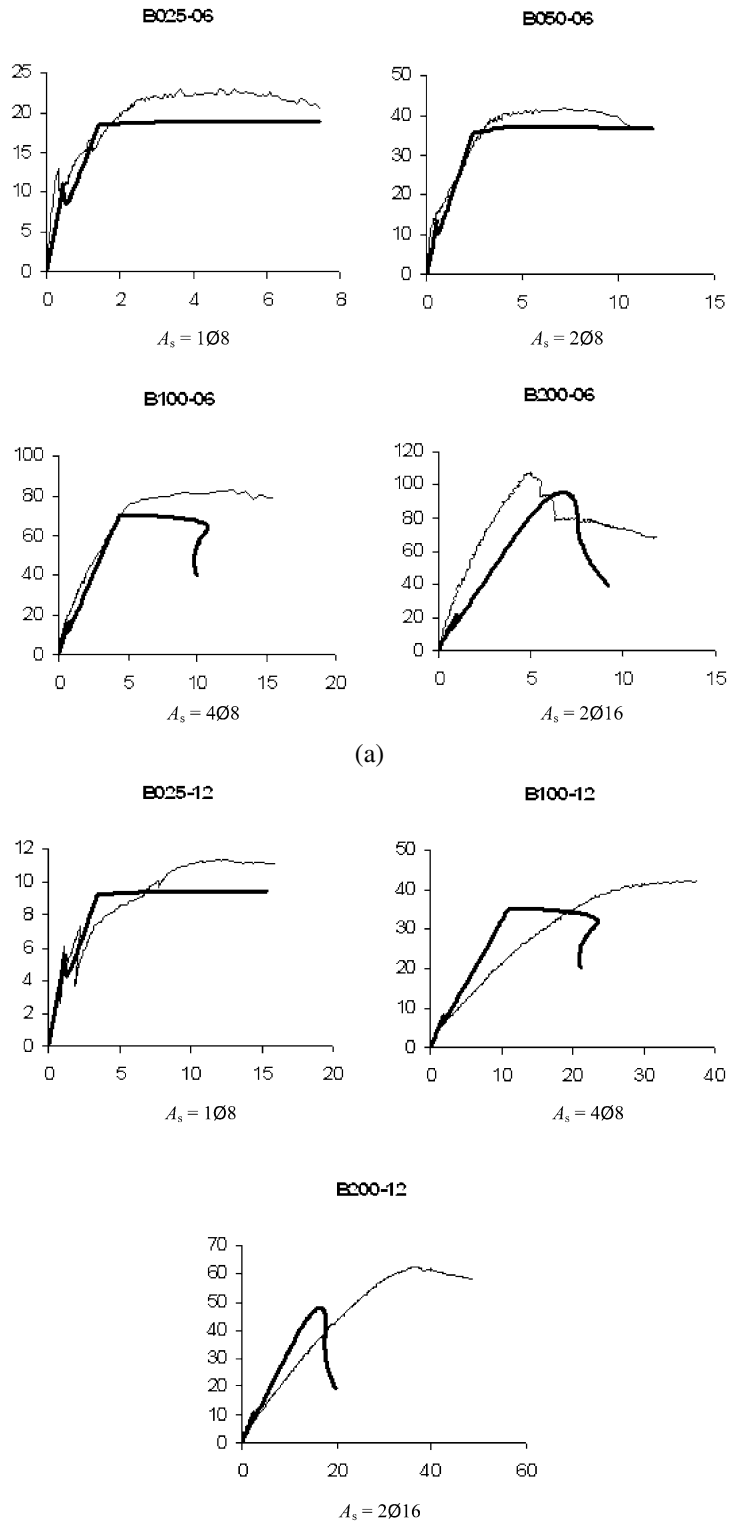

Fig. 8 Numerical (thicker curve) vs. experimental P [kN]–δ [mm] curves for specimens size B: (**a**) $l/h = 6$; (**b**) $l/h = 12$

crete having an average compressive strength equal to 40 MPa. The curves in Figs. 7–9 evidence a general good agreement between numerical and experimental results. However, it has to be emphasized that the hypothesis of sectional localization characterizing the proposed model becomes less consistent with the real mechanical behaviour of RC beams in the case of high steel percentages where, indeed, the fracture phenomenon is more spread along the beam length.

For this reason, most of the experimental curves show a nearly linear-elastic branch, up to the first cracking load, followed by a second inclined branch due to a decrease in the tensile stiffness due to the cracking phenomenon.

Figures 7–9 represent the experimental vs. numerical comparison.

Depending on the reinforcement percentage, it is possible to observe a transition from a pure flexural

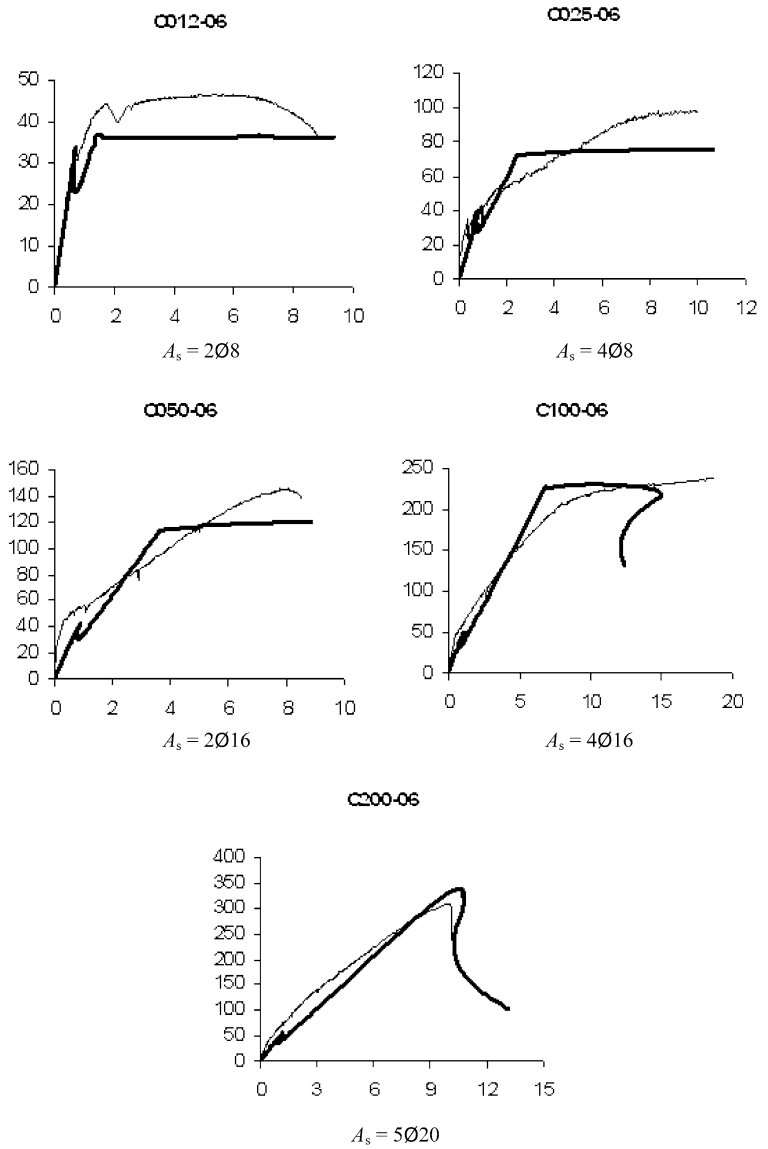

(a)

Fig. 9 Numerical (*thicker curve*) vs. experimental P [kN]–δ [mm] curves for specimens size C: (**a**) $l/h = 6$; (**b**) $l/h = 12$; (**c**) $l/h = 18$

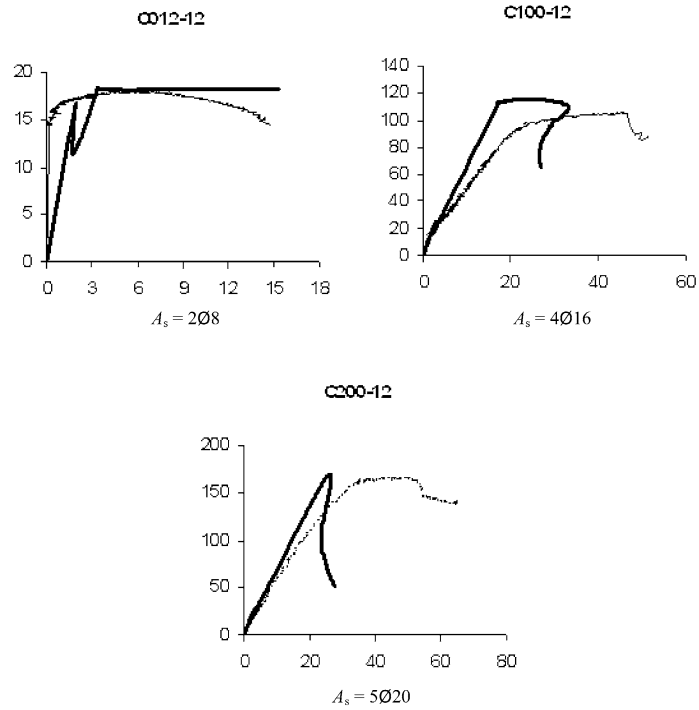

(b)

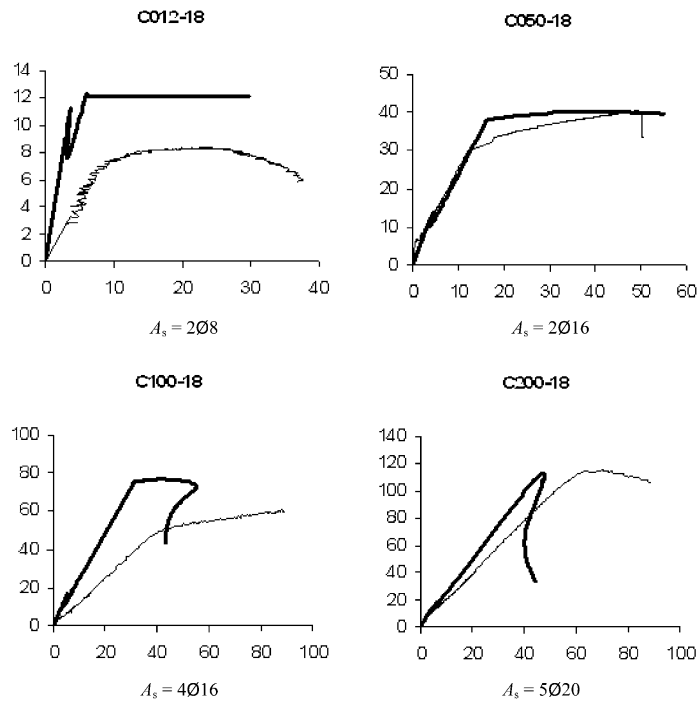

(c)

Fig. 9 (*Continued*)

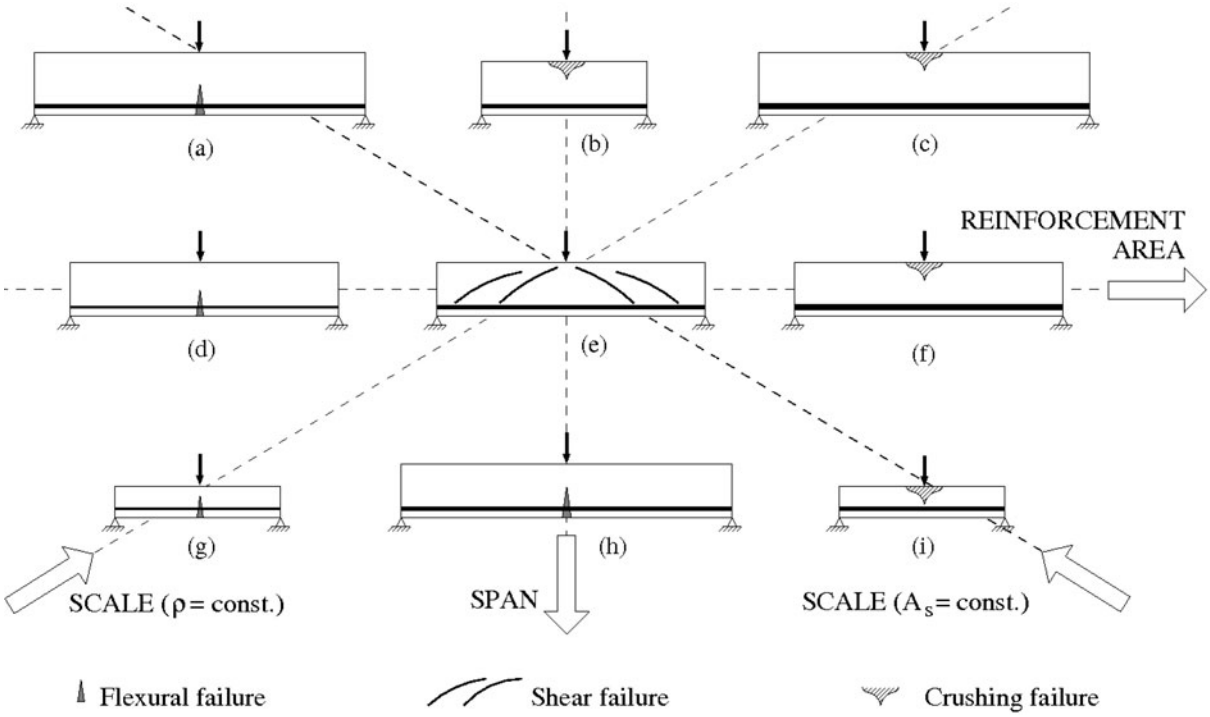

Fig. 10 Fundamental collapse mechanisms of RC beams

collapse to a crushing collapse of concrete in compression. In general, for low reinforcement percentages, such as $\rho = 0.12$ %, 0.25 % and 0.50 %, steel yielding precedes crushing of concrete in compression. The first peak in the moment, M, vs. rotation, ϕ, curve corresponds to the first crack formation, the concrete tensile strength being reached, while the second peak corresponds to steel yielding, which is always followed by a plastic plateau. On the other hand, for high reinforcement percentages, such as $\rho = 1.00$ % and 2.00 %, crushing of concrete in compression precedes steel yielding in tension. In this cases, in fact, the moment, M, vs. rotation, ϕ, curves show a descending branch that indicates the crushing phenomenon. Some cases, e.g. size A, $\lambda = 18$ and $\rho = 2.0$ %, show an elastic-perfectly brittle behaviour, in fact, after the peak load is reached, the response shows a sudden drop in the load carrying capacity with a definitive collapse for concrete crushing in compression without the reinforcement is yielding.

The load-deflection diagrams have evidenced that, for constant slenderness and reinforcement percentage, the peak load and displacement increase by increasing the beam size-scale. On the other hand, for constant size and reinforcement percentage, by increasing the beam slenderness, the peak-load displacement increases whereas the peak load decreases, moreover the behaviour appearing sensibly more ductile.

5 Discussion and conclusions

The integrated Cohesive/Overlapping model is applied to the study of the flexural behaviour of reinforced concrete beams by interpreting the results available from an experimental investigation proposed by the ESIS Technical Committee 9 on Concrete [6, 9]. The aim of the research was to give a rational and unified explanation to the transitions usually observable between collapse mechanisms of RC beams in flexure.

Reinforced concrete beams undergo different failure mechanisms by varying steel percentage and/or beam slenderness and/or beam size-scale (see Fig. 10). Three fundamental collapse mechanisms are foreseen:

– nucleation and propagation of cracks at the edge in tension (flexural failure);
– crushing at the edge in compression (crushing failure);

Table 6 Failure mechanisms of the tested beams (® rupture of reinforcement under low displacements; □ rupture of reinforcement under high displacements; O collapse of concrete with a smooth peak; Δ peak at a low displacement and crushing of concrete; © error of the test (high reinforcement percentage); T shear collapse)

A012-06	®	B200-06	Δ
A025-06	□	B025-12	□
A100-06	O	B100-12	O
A200-06	Δ	B200-12	O
A012-12	□	C012-06	□
A025-12	□	C025-06	□
A050-12	O	C050-06	O
A100-12	O	C100-06	T
A200-12	Δ	C200-06	T
A025-18	□	C012-12	□
A050-18	O	C100-12	T
A100-18	O	C200-12	Δ
A200-18	©	C012-18	□
B025-06	□	C050-12	O
B050-06	O	C100-18	O
B100-06	O	C200-18	Δ

– formation of inclined shear cracks (shear failure).

In particular, for a constant size and by increasing the reinforcement percentage, it has been verified the existence of a transitional failure process which from ductile has become brittle. In fact, by increasing the steel content a collapse transition occurs, which moves from the tensile to the compressive edge.

Table 6 shows the type of rupture occurred for each beam.

The experimental vs. numerical comparisons demonstrate that the proposed model can be successfully applied to the study of reinforced concrete, revealing the influence of size-scale, reinforcement percentage, and slenderness in the mechanical behaviour of the beams in flexure.

References

1. Baluch M, Azad A, Ashmawi W (1992) Fracture mechanics application to reinforced concrete members in flexure. In: Carpinteri A (ed) Applications of fracture mechanics to reinforced concrete. Elsevier, London, pp 413–436
2. Bažant ZP (1989) Identification of strain-softening constitutive relation from uniaxial tests by series coupling model for localization. Cem Concr Res 19:973–977
3. Bazant ZP, Beisel S (1994) Smeared-tip superposition method for cohesive fracture with rate effect and creep. Int J Fract 65:277–290
4. Bosco C, Carpinteri A (1992) Softening and snap-through behavior of reinforced elements. J Eng Mech 118:1564–1577
5. Bosco C, Carpinteri A (1992) Fracture mechanics evaluation of minimum reinforcement in concrete structures. In: Carpinteri A (ed) Applications of fracture mechanics to reinforced concrete. Elsevier, London, pp 347–377
6. Bosco C, Carpinteri A (1993) Scale effects and transitional phenomena of reinforced concrete beams in flexure. ESIS Technical Committée 9 Round Robin proposal, Department of Structural Engineering of Politecnico di Torino, Italy
7. Bosco C, Carpinteri A (1995) Discontinuous constitutive response of brittle matrix fibrous composites. J Mech Phys Solids 43:261–274
8. Bosco C, Carpinteri A, Debernardi PG (1990) Minimum reinforcement in high-strength concrete. J Struct Eng 116:427–437
9. Bosco C, Carpinteri A, Ferro G, El-Khatieb M (1996) Scale effects and transitional failure phenomena of reinforced concrete beams in flexure. Report to ESIS Technical Committée 9, Dipartimento di Ingegneria Strutturale, Politecnico di Torino
10. Brincker R, Henriksen MS, Christensen FA, Heshe G (1999) Size effects on the bending behaviour of reinforced concrete beams. In: Carpinteri A (ed) Minimum reinforcement in concrete members. Elsevier, Oxford, pp 127–180
11. Carpinteri A (1980) Size effect in fracture toughness testing: a dimensional analysis approach. In: Sih GC, Mirabile M (eds) Analytical and experimental fracture mechanics. Sijthoff & Noordhoff, Alphen an den Rijn, pp 785–797
12. Carpinteri A (1981) A fracture mechanics model for reinforced concrete collapse. In: Advanced mechanics of reinforced concrete, Proc IABSE colloquium. Delft University Press, Delft, pp 17–30
13. Carpinteri A (1981) Static and energetic fracture parameters for rocks and concretes. Mater Struct 14:151–162
14. Carpinteri A (1982) Notch sensitivity in fracture testing of aggregative materials. Eng Fract Mech 16:467–481
15. Carpinteri A (1984) Stability of fracturing process in RC beams. J Struct Eng 110:544–558
16. Carpinteri A (1985) Interpretation of the Griffith instability as a bifurcation of the global equilibrium. In: Shah SP (ed) Application of fracture mechanics to cementitious composites. Nijhoff, Dordrecht, pp 287–316
17. Carpinteri A, Massabò R (1996) Bridged versus cohesive crack in the flexural behaviour of brittle-matrix composites. Int J Fract 81:125–145
18. Carpinteri A, Colombo G, Ferrara G, Giuseppetti G (1989) Numerical simulation of concrete fracture through a bilinear softening stress-crack opening displacement law. In: Shah SP, Swartz SE (eds) Fracture of concrete and rock. Springer, New York, pp 131–141
19. Carpinteri A, Ferro G, Ventura G (2003) Size effects on flexural response of reinforced concrete elements with nonlinear matrix. Eng Fract Mech 70:995–1013
20. Carpinteri A, Ruiz Carmona J, Ventura G (2007) Propagation of flexural and shear cracks through reinforced concrete beams by the bridged crack model. Mag Concr Res 59:743–756

21. Carpinteri A, Corrado M, Paggi M, Mancini G (2007) Cohesive versus overlapping crack model for a size effect analysis of RC elements in bending. In: Carpinteri A, Gambarova P, Ferro G, Plizzari G (eds) Fracture mechanics of concrete and concrete structures. Taylor & Francis, Leiden, pp 655–663
22. Carpinteri A, Corrado M, Paggi M, Mancini G (2009) New model for the analysis of size-scale effects on the ductility of reinforced concrete elements in bending. J Eng Mech 135:221–229
23. Comité Euro-International du Béton C (1993) CEB-FIP Model Code 1990, Bulletin No. 213/214. Telford, Lausanne
24. Corrado M, Cadamuro E, Carpinteri A (2011) Dimensional analysis approach to study snap back-to-softening-to-ductile transitions in lightly reinforced quasi-brittle materials. Int J Fract 172:53–63
25. El-Khatieb M (1997) Transizione di scala duttile-fragile per le travi in calcestruzzo armato. PhD Thesis, Dipartimento di Ingegneria Strutturale, Politecnico di Torino
26. Eurocode 2 (2004) Design of concrete structures, Part 1-1: General rules and rules for buildings. p 230
27. Gustafsson PJ (1985) Fracture mechanics studies of non-yielding materials like concrete. Report TVBM-1007, Div Bldg Mater Lund Inst Tech, Sweden
28. Gustafsson PJ, Hillerborg A (1988) Sensitivity in shear strength of longitudinally reinforced concrete beams to fracture energy of concrete. ACI Struct J 85:286–294
29. Hawkins NM, Hjorsetet K (1992) Minimum reinforcement requirement for concrete flexural members. Elsevier, London, pp 379–412
30. Hillerborg A (1990) Fracture mechanics concepts applied to moment capacity and rotational capacity of reinforced concrete beams. Eng Fract Mech 35:233–240
31. Hillerborg A, Modeer M, Petersson PE (1976) Analysis of crack formation and crack growth in concrete by means of fracture mechanics and finite elements. Cem Concr Res 6:773–782
32. Irwin GR (1957) Analysis of stresses and strains near the end of a crack traversing a plate. J Appl Mech 24:361–364
33. Jansen DC, Shah SP (1997) Effect of length on compressive strain softening of concrete. J Eng Mech 123:25–35
34. Jenq YS, Shah SP (1989) Shear resistance of reinforced concrete beams—a fracture mechanics approach. In: Li VC, Bazant ZP (eds) Fracture mechanics: application to concrete (Special Report ACI SP-118). Am Concrete Institute, Detroit, pp 327–358
35. Markeset G, Hillerborg A (1995) Softening of concrete in compression localization and size effects. Cem Concr Res 25:702–708
36. Palmquist SM, Jansen DC (2001) Postpeak strain-stress relationship for concrete in compression. ACI Mater J 98:213–219
37. Planas J, Elices M (1992) Asymptotic analysis of a cohesive crack: 1. Theoretical background. Int J Fract 55:153–177
38. RILEM TCS (1985) Determination of the fracture energy of mortar and concrete by means of three-point bend tests on notched beams. Draft Recommendation. Materials and Structures, vol 18
39. Ruiz G (2001) Propagation of a cohesive crack crossing a reinforcement layer. Int J Fract 111:265–282
40. Ruiz G, Elices M, Planas J (1999) Size effects and bond-slip dependence of lightly reinforced concrete beams. In: Carpinteri A (ed) Minimum reinforcement in concrete members. Elsevier, Oxford, pp 127–180
41. So KO, Karihaloo BL (1993) Shear capacity of longitudinally reinforced beams—a fracture mechanics approach. J ACI 90:591–600
42. Suzuki M, Akiyama M, Matsuzaki H, Dang TH (2006) Concentric loading test of RC columns with normal- and high-strength materials and averaged stress-strain model for confined concrete considering compressive fracture energy. In: Proc 2nd fib congress, Naples, Italy
43. UNI 6556 Determinazione del modulo elastico secante a compressione
44. van Vliet M, van Mier J (1996) Experimental investigation of concrete fracture under uniaxial compression. Mech Cohes-Frict Mater 1(1):115–127